Comparison of a Modal Method and a Proper Orthogonal Decomposition approach for multi-group time-dependent reactor spatial kinetics

Alberto Sartori [a], Davide Baroli [b], Antonio Cammi [a], Davide Chiesa [d,e], Lelio Luzzi [a,*], Roberto Ponciroli [a], Ezio Previtali [d], Marco Enrico Ricotti [a], Gianluigi Rozza [c], Monica Sisti [d,e]

[a] *Politecnico di Milano, Department of Energy, CeSNEF (Enrico Fermi Center for Nuclear Studies), Via Ponzio 34/3, 20133 Milano, Italy*
[b] *Politecnico di Milano, Department of Mathematics, MOX (Modelling and Scientific Computing), Via Bonardi 9, 20133 Milano, Italy*
[c] *SISSA (International School for Advanced Studies), mathLab, Via Bonomea 265, 34136 Trieste, Italy*
[d] *INFN (Istituto Nazionale di Fisica Nucleare), Section of Milano Bicocca, Piazza della Scienza 3, 20126 Milano, Italy*
[e] *Università degli Studi di Milano Bicocca, Physics Department, Piazza della Scienza 3, 20126 Milano, Italy*

Received 30 September 2013
Received in revised form 26 March 2014
Accepted 31 March 2014

1. Introduction

In the development of the control systems, the preliminary stage of modelling mainly concerns the correct evaluation of the representative system time constants, and getting the fundamental aspects related to the plant response to the outside perturbations. For this reason, in control oriented simulators, the model is usually based on non-linear systems of Differential–Algebraic Equations (DAEs), expressed by $\dot{\mathbf{x}} = \mathbf{f}(t, \mathbf{x}, \mathbf{z})$. Indeed, the system of Ordinary Differential Equations (ODEs) for $\mathbf{x}(t)$ depends on additional variables and the solution is forced to satisfy algebraic constraints $\mathbf{0} = \mathbf{g}(t, \mathbf{x}, \mathbf{z})$ (Ascher and Petzold, 1997). In many cases, it is sufficient to employ simplified lumped parameter models, which neglect the spatial dependence of the variables, studying only the average behavior of the system and its temporal evolution. In addition, these systems of differential equations can be easily linearized in order to study the system behavior close to a given operating condition. In this way, it is possible to use the tools of linear analysis, which allow achieving effective solutions that can be applied to the original non-linear models. For these reasons, in the analysis of the nuclear reactor dynamics, the most diffused approach is constituted by the *Point-Kinetics* (PK) equations (Schultz, 1961). This description of the neutronics is based on a set of coupled non-linear ODEs that describe both the time-dependence of the neutron population in the reactor and the decay of the delayed neutron precursors, allowing for the main feedback reactivity effects. Among the several assumptions entered in the derivation of these equations, the strongest approximation regards the shape of the neutron flux, which is assumed to be represented by a single, time-independent spatial mode. Indeed, it is common to adopt a shape function characterizing a critical core configuration if the reactor is close to the critical state or on a truly asymptotic period. When the changes in core composition are sufficiently slow, an instantaneous steady-state criticality calculation of the shape function can be performed, even though this shape will slowly change with time. Such a scheme is known as the *adiabatic approximation* (Duderstadt and Hamilton, 1976).

Otherwise, whether the reactors are characterized by complex geometries and asymmetric core configurations, more accurate

* Corresponding author. Tel.: +39 02 2399 6326; fax: +39 02 2399 6309.
E-mail address: lelio.luzzi@polimi.it (L. Luzzi).

Nomenclature

Latin symbols

b_i^g	ith generic spatial basis function of the gth energy group [$m^{-2}\ s^{-1}$]
C_m	concentration of the mth precursor group [m^{-3}]
D_g	neutron diffusion coefficient in the gth energy group [m]
g	refers to the considered energy group ($g = 1$ for the fast group, $g = 2$ for the thermal group)
N	number of the employed basis functions [–]
N_s	number of the computed snapshots [–]
m	subscript referring to the precursor groups ($m = 1, \ldots, 8$)
P	thermal power [W]
$\mathbf{r}$	spatial coordinate [m]
t	time [s]
u_i^g	ith POD basis functions of the gth energy group [$m^{-2}\ s^{-1}$]
v_g	neutron speed of the gth energy group [$m\ s^{-1}$]
$w_f^{(l)}$	recoverable thermal energy per fission event for the l-isotope [J]

Greek symbols

β	total delayed neutron fraction [–]
β_m	delayed neutron fraction of the mth precursor group [–]
η_i	normalized concentration of the ith precursor group [–]
λ_i	ith eigenvalue [–]
λ_m	decay constant of the mth precursor group [s^{-1}]
Λ	prompt neutron generation time [s]
ν	average number of neutrons emitted per fission [–]
ρ	system reactivity [pcm]
Σ	macroscopic cross-section [m^{-1}]
Σ_a^g	macroscopic absorption cross-section in the gth energy group [m^{-1}]
Σ_f^g	macroscopic fission cross-section in the gth energy group [m^{-1}]
$\Sigma_s^{g\to g'}$	macroscopic group transfer cross-section from energy group g to g' [m^{-1}]
Φ_g	neutron flux in the gth energy group [$m^{-2}\ s^{-1}$]
χ_d^g	fraction of delayed neutrons generated in the gth energy group [–]
χ_p^g	fraction of prompt neutrons generated in the gth energy group [–]
ψ_i^g	ith spatial eigenfunction of the neutron flux in the gth energy group [$m^{-2}\ s^{-1}$]
Ψ	normalized thermal power [–]
Ω	spatial domain [m^2]

Acronyms

BC	Boundary Conditions
DAE	Differential Algebraic Equation
MM	Modal Method
MP	Multi-Physics
MUMPS	MUltifrontal Massively Parallel sparse direct Solver
ODE	Ordinary Differential Equation
PK	Point Kinetics
POD	Proper Orthogonal Decomposition
SVD	Singular Value Decomposition

modelling approaches may provide more detailed insights concerning the reactor behavior during operational transients. It is worth mentioning that innovative reactor concepts, for instance Generation IV reactors (GIF, 2002), feature power density and temperature ranges, experienced by structural materials, such that the corresponding spatial dependence cannot be neglected. At the state of the art, a more complete approach, which takes into account the coupling among the neutronics with the other physics, is given by the Multi-Physics (MP) approach (see e.g., Cammi et al., 2011; Aufiero et al., 2013), where all the involved physics are simulated within the same computational environment. The main drawback of the MP is that the computational burden is quite high, and simulating the entire core turns out to be very demanding in terms of computational costs. In addition, it is quite difficult to get the system governing dynamics and then set up a simulation tool that may assess and represent the dynamic response of the overall system at different operating conditions.

It is therefore necessary to develop a sufficiently accurate description of the reactor core spatial dynamics, based on a set of ODEs to be employed in a control-oriented simulator. To this aim, in the present paper, the capabilities of two approaches – the *Modal Method* (MM) (Stacey, 1969; Xia et al., 2012) and one based on the *Proper Orthogonal Decomposition* (POD) (Holmes et al., 1996; Chatterjee, 2000; Liang et al., 2002; Buchan et al., 2013) technique – are compared on a 2D domain. The comparison focuses on the capability of the two approaches of reproducing both the reactivity and the neutron flux shape for different reactor configuration, with reference to a TRIGA Mark II reactor (General Atomic, 1964). Such reactor has been selected as case study because it is a pool-type reactor, whose core features a non-symmetric configuration, beside being cooled with water in natural convection. Moreover, the simulation outcomes will be assessed, in a future work, by means of collected experimental data. However, the main focus of the present paper is the comparison of the above mentioned MM and POD approaches to find out the right track to be pursued in the future. Therefore, since this study is more concerned on the modelling approaches, rather than the reactor model itself, the geometry of the reactor has been taken 2D to speed up the computational time.

The MM approach was theorized in the sixties (Stacey, 1969) but it was not systematically employed because of the high computational burden for the determination of the higher order eigenfunctions of a reactor core. The MM, basically, approximates a function by means of a linear combination of its eigenfunctions. Nowadays, in literature it is possible to find many attempts in developing non-zero dimensional reactor models for different applications by means of modal synthesis method. For a review of the works carried out in the nuclear engineering field, the reader may refer to Xia et al. (2012).

Similarly to the MM, the POD was not recently theorized (Pearson, 1901) but it was not widely exploited until the advent of electronic computers. The POD is a reduction order technique aimed at obtaining the most characteristic structure of the problem using a low-dimensional approximate descriptions of a high-dimensional process (Quarteroni et al., 2011). Applications of POD include image processing, data compression, signal analysis, modelling and control of chemical reaction systems, turbulence models, coherent structures in fluids, control of fluids and electrical power grids. In the nuclear engineering field, POD has not been extensively employed, even though its potentialities have been underlined, e.g., (Merzari and Ninokata, 2011 and Prill and Class, 2014) to name a few. In literature, examples of the application of

POD to neutronics can be found in Wols (2010) and Buchan et al. (2013). The former presents a POD-based reduced order model for the mono-energetic generalized eigenvalue equation, which is associated to the neutron diffusion equation in the steady state condition. In the latter, the multi-group time-dependent neutron flux is approximated as a linear combination of α-eigenfunctions, while the POD is briefly addressed and not applied to the time-dependent problem. The study reported in the present paper shares some aspects with the work of Wols (2010) and such approach has been further improved. Indeed, for the first time, the POD capabilities are exploited for solving the multi-group time-dependent neutron diffusion equation by training the POD basis to handle localized perturbations, as it will be suitably explained in Section 4. In particular, two opportunities of POD approach have been exploited: the primal Galerkin projection onto a low dimensional space, which is spanned by the so-called most energetic basis (Merzari and Ninokata, 2011), and off-line/on-line decomposition strategies, which allow achieving small calculation cost for a high performance in real-time simulation. As a major outcome, there is a great saving in on-line computation for each input–output evaluation of the quantities of interest, while an increase of preprocessing (off-line) calculation has to be dealt with (Rozza et al., 2008).

The paper is organized as follows. Section 2 presents the reactor chosen as case study and its modelling. The MM and the POD approaches are described in Sections 3 and 4, respectively. In Section 5, the Inverse Method used to compute the reactivity according to the two approaches is presented. Subsequently, the comparison between the MM and POD results is detailed in Section 6. Finally, the main conclusions and the next steps to be taken are drawn in Section 7.

2. Modelling

The TRIGA Mark II reactor of the University of Pavia (Italy) has been chosen as case study. The TRIGA is a research thermal reactor cooled with water circulating in natural convection. Fig. 1 shows the map of the core, which features three control rods (SHIM, TRANSIENT, REGULATING), two irradiation channels (C.T., RABBIT), and one channel where the source for the start-up of the reactor is placed surrounded by two elements of graphite (DUMMY). All other elements are fuel pins.

In order to describe the neutron kinetics the multi-group diffusion theory (Duderstadt and Hamilton, 1976), with two energy groups and eight group of precursors (C_m) has been employed. In equations, it reads:

$$\underline{\underline{V}}^{-1}\frac{\partial \underline{\Phi}}{\partial t} = \nabla\cdot\left(\underline{\underline{D}}\nabla\underline{\Phi}\right) - \underline{\underline{\Sigma_a}}\underline{\Phi} - \underline{\underline{\Sigma_s}}\underline{\Phi} + (1-\beta)\underline{\chi_p}\underline{F}^T\underline{\Phi} + \\ + \sum_m \lambda_m \underline{\chi_d} C_m, \tag{1}$$

$$\frac{\partial C_m}{\partial t} = -\lambda_m C_m + \beta_m \underline{F}^T\underline{\Phi} \quad \text{for} \quad m = 1,\ldots,8, \tag{2}$$

with a given initial condition

$$\underline{\Phi}(t=0) = \underline{\Phi_0} \quad \text{and} \quad C_m(t=0) = C_m^0, \tag{3}$$

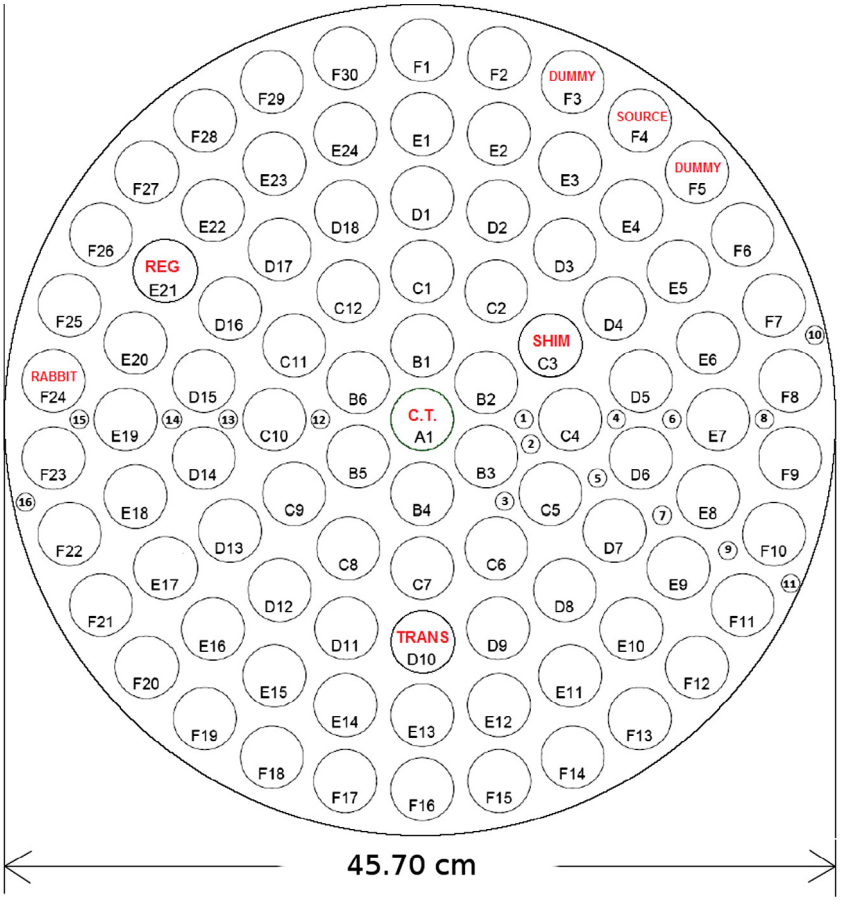

Fig. 1. Map of the TRIGA Mark II reactor core.

where

$$\begin{cases} \underline{\Phi} = \begin{bmatrix} \Phi_1(\mathbf{r},t) \\ \Phi_2(\mathbf{r},t) \end{bmatrix}, \\ \underline{\underline{V^{-1}}} = \begin{bmatrix} \frac{1}{v_1}(\mathbf{r}) & 0 \\ 0 & \frac{1}{v_2}(\mathbf{r}) \end{bmatrix}, \\ \underline{\underline{D}} = \begin{bmatrix} D_1(\mathbf{r}) & 0 \\ 0 & D_2(\mathbf{r}) \end{bmatrix}, \\ \underline{\underline{\Sigma_a}} = \begin{bmatrix} \Sigma_a^1(\mathbf{r}) & 0 \\ 0 & \Sigma_a^2(\mathbf{r}) \end{bmatrix}, \\ \underline{\underline{\Sigma_s}} = \begin{bmatrix} \Sigma_s^{1\to 2}(\mathbf{r}) & -\Sigma_s^{2\to 1}(\mathbf{r}) \\ -\Sigma_s^{1\to 2}(\mathbf{r}) & \Sigma_s^{2\to 1}(\mathbf{r}) \end{bmatrix}, \\ \underline{\chi_p} = \begin{bmatrix} \chi_p^1 \\ \chi_p^2 \end{bmatrix}, \\ \underline{F}^T = \begin{bmatrix} \nu\Sigma_f^1(\mathbf{r}) & \nu\Sigma_f^2(\mathbf{r}) \end{bmatrix}, \\ \underline{\chi_d} = \begin{bmatrix} \chi_d^1 \\ \chi_d^2 \end{bmatrix}. \end{cases} \tag{4}$$

2.1. Neutronic input generation with SERPENT

The neutronic parameters ($\underline{\underline{V^{-1}}}, \underline{\underline{D}}, \underline{\underline{\Sigma_a}}, \underline{\underline{\Sigma_s}}, \underline{\chi_p}, \underline{F}^T, \underline{\chi_d}$) have been generated by means of the continuous energy Monte Carlo neutron transport code SERPENT (SERPENT, 2011), which features group constant generation capabilities, using the nuclear data library JEFF 3.1 (Koning et al., 2006). As far as the SERPENT model is concerned, the core and the pin geometries are represented, respectively, in Figs. 2 and 3. All the fuel pins have been taken into account with the surrounding cladding, the two irradiation channels have been considered empty (filled with air), whereas, for the sake of simplicity, the control rods, the dummy elements and the source have been "replaced" with water. The isotopic composition of the input materials is provided in Table 1.

The group constants have been obtained after runs of 10 millions active neutron histories. Simulations consist of 500 active cycles of $2 \cdot 10^4$ neutrons, leading to a standard deviation lower than 3% for all the computed parameters.[1] Fifty inactive cycles are adopted to allow the convergence of the fission source distribution employed for the active cycles. When the neutronic parameters for the void have been generated, the air has been homogenized with the surrounding water ensuring that the diffusion approximation holds. In addition, for the sake of simplicity, the fuel pins have been homogenized with the cladding and the coolant. The parameters generated, which have been used as input for both the MM and POD approaches, are reported in Table 2.

The homogeneous Dirichlet Boundary Conditions (BC) have been set, which lead to a good approximation of flux shape and reactivity value. Indeed, the core is surrounded by a ring of reflector of graphite, which improves the neutron thermalization. This leads to a small increase of the thermal flux near the border that cannot be taken into account with the employed BC. Therefore, the flux shape is correctly evaluated throughout the core, except near the external border. Since this work is more focused on the comparison of the two approaches, rather than on the development of an accurate model of the reactor, the adoption of such BC may be still considered acceptable.

2.2. Deriving the system of ODEs

In order to derive the system of ODEs, which describes the reactor kinetics, the flux has been approximated as follows:

[1] Thanks to the reduced values of the obtained standard deviations, performing an uncertainty propagation has not been considered necessary.

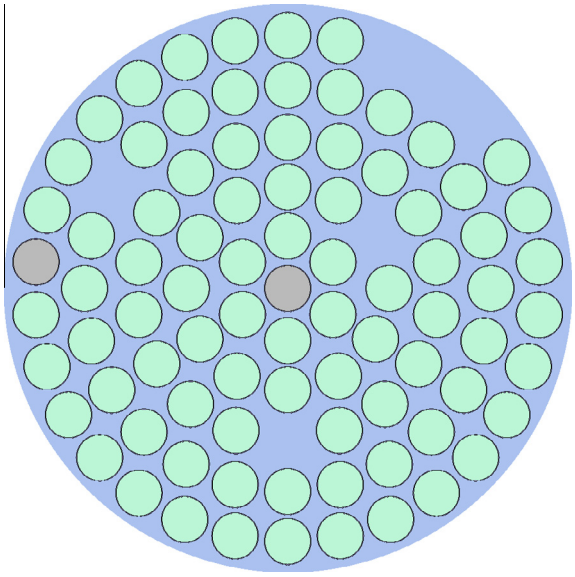

Fig. 2. Geometry employed in SERPENT code for representing the system configuration.

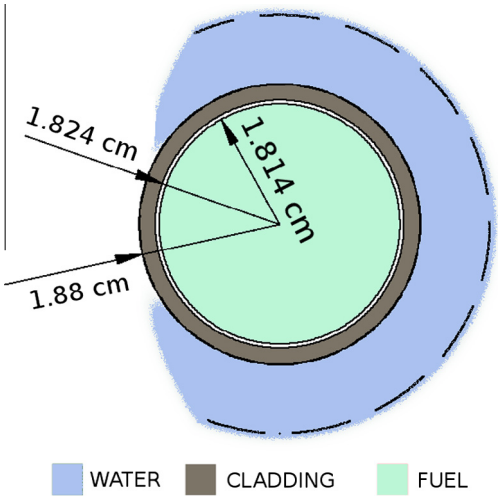

Fig. 3. Geometry of the pin employed in SERPENT code.

Table 1
Isotopic composition of the SERPENT input materials.

Fuel		Cladding		Water	
Isotope	wt%	Isotope	wt%	Isotope	atomic ratio
U-235	1.607	V-nat	0.10	O-16	1.0
U-238	6.531	Cr-nat	0.02	H-1	2.0
Zr-nat	90.836	Mn-nat	0.01		
H-1	1.026	Fe-nat	0.10	Air	
		Al-27	99.57	Isotope	wt%
		Cu-nat	0.10	O-16	10.0
		Ga-nat	0.10	N-14	90.0

$$\underline{\Phi} \simeq \sum_{i=1}^{N} \underline{\underline{b_i}}\, \underline{a_i}(t), \tag{5}$$

where

Table 2
Neutronic parameters generated by the SERPENT code.

Parameter	Fuel	Water	Void
D_1 [m]	$8.77 \cdot 10^{-3}$	$8.51 \cdot 10^{-3}$	$3.82 \cdot 10^{-2}$
D_2 [m]	$1.92 \cdot 10^{-3}$	$1.39 \cdot 10^{-3}$	$7.13 \cdot 10^{-3}$
Σ_a^1 [m^{-1}]	$4.85 \cdot 10^{-1}$	$5.04 \cdot 10^{-2}$	$1.23 \cdot 10^{-2}$
Σ_a^2 [m^{-1}]	7.53	1.70	$4.18 \cdot 10^{-1}$
Σ_f^1 [m^{-1}]	$3.15 \cdot 10^{-1}$	–	–
Σ_f^2 [m^{-1}]	$1.08 \cdot 10^{1}$	–	–
$\Sigma_s^{1\to2}$ [m^{-1}]	3.04	5.34	$9.08 \cdot 10^{-1}$
$\Sigma_s^{2\to1}$ [m^{-1}]	$3.21 \cdot 10^{-2}$	$2.49 \cdot 10^{-2}$	$1.18 \cdot 10^{-2}$
$1/v_1$ [s/m]	$5.87 \cdot 10^{-6}$	$7.58 \cdot 10^{-6}$	$6.58 \cdot 10^{-6}$
$1/v_2$ [s/m]	$3.00 \cdot 10^{-4}$	$3.47 \cdot 10^{-4}$	$3.30 \cdot 10^{-4}$
χ_p^1 [–]	1.0	–	–
χ_p^2 [–]	0.0	–	–
χ_d^1 [–]	1.0	–	–
χ_d^2 [–]	0.0	–	–

$$\begin{cases} \underline{\underline{b_i}} = \begin{bmatrix} b_i^1(\mathbf{r}) & 0 \\ 0 & b_i^2(\mathbf{r}) \end{bmatrix}, \\ \underline{a_i}(t) = \begin{bmatrix} a_i^1(t) \\ a_i^2(t) \end{bmatrix}. \end{cases} \tag{6}$$

In Eq. (5), $\{\underline{\underline{b_i}}\}$ is a spatial basis where the flux is projected, and $a_i(t)$ are the time-dependent coefficients, which are the unknowns of the obtained ODEs system. In this work, two spatial bases have been considered, one generated by the eigenfunctions associated to Eq. (1) (MM approach), and one generated by means of the POD technique.

Once Eqs. (1) and (2) are projected onto the corresponding spatial basis, the following equations for $j = 1, \ldots, N$ are obtained for both approaches:

$$\sum_{i=1}^{N} \underline{\underline{\tau_{ji}}}\, \dot{\underline{a_i}}(t) = \sum_{i=1}^{N} \left[\underline{\underline{A_{ji}}}\, \underline{a_i}(t) + (1-\beta) \underline{\underline{F_{p,ji}}}\, \underline{a_i}(t) \right] + \tag{7}$$
$$+ \sum_{m=1}^{8} \lambda_m \underline{C_{mj}}(t),$$

$$\dot{\underline{C_{mj}}}(t) = -\lambda_m \underline{C_{mj}}(t) + \beta_m \sum_{i=1}^{N} \underline{\underline{F_{d,ji}}}\, \underline{a_i}(t) \text{ for } m = 1, \ldots, 8, \tag{8}$$

where the expressions for the parameters $\underline{\underline{\tau_{ji}}}$, $\underline{\underline{A_{ji}}}$, $\underline{\underline{F_{p,ji}}}$, $\underline{C_{mj}}$, $\underline{\underline{F_{d,ji}}}$ will be given in Sections 3 and 4 for the MM and POD approach, respectively. The $a_i(t)$ coefficients can be computed integrating in time the above system of ODEs starting from a given initial condition. In particular, the stiff solver ode15s provided by MATLAB® and SIMULINK® software (2005) has been employed.

The needed calculations for the definition of the two spatial bases have been performed using the finite element method (Quarteroni and Valli, 2008). The mesh employed (Fig. 4) features a 2D geometry using tri-noded triangular elements, where, for the sake of simplicity, all the fuel pins have been homogenized and only the two irradiation channel regions have been taken separated.

3. Modal Method approach

The essential feature of Modal Methods is spanning the expansion of spatial modes generated from the reference configuration, which is described by the non symmetric generalized eigenvalue problem associated to Eq. (1), namely:

$$(-\nabla \cdot \underline{\underline{D}} \nabla + \underline{\underline{\Sigma_a}} + \underline{\underline{\Sigma_s}}) \underline{\psi_i} = \lambda_i \underline{\chi_p} \underline{F}^T \underline{\psi_i}, \tag{9}$$

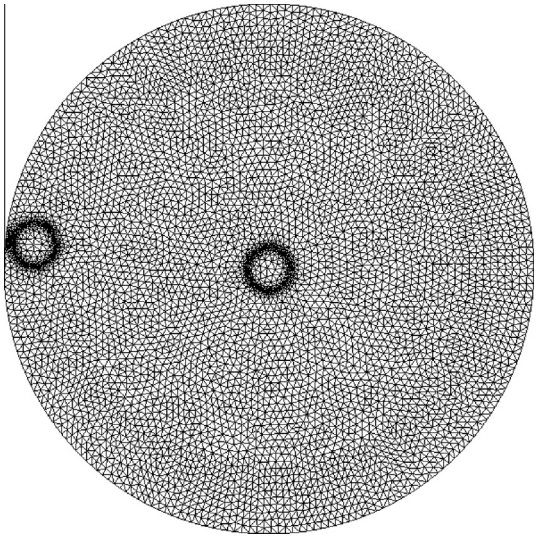

Fig. 4. Mesh employed for the finite element calculations.

where the eigenfunctions are listed in ascending order starting from the *minimum* eigenvalue. The first eigenfunctions of each group $\underline{\psi_0}$ give the fundamental flux distribution. The core criticality condition is determined by the inverse of λ_0.

The former equation can be rewritten in the operator theory context as follows:

$$\mathcal{L} \underline{\psi_i} = \lambda_i \mathcal{M} \underline{\psi_i}, \tag{10}$$

where the operators denoted in (10) are the neutronic removal operator $\mathcal{L} = (-\nabla \cdot \underline{\underline{D}} \nabla + \underline{\underline{\Sigma_a}} + \underline{\underline{\Sigma_s}})$ and the production operator $\mathcal{M} = \underline{\chi_p} \underline{F}^T$. Because of the non-Hermitian nature of operator $\mathcal{L}$, the adjoint generalized problem associated to Eq. (9) has to be solved, in order to obtain the bi-orthogonal adjoint eigenvectors $\underline{\psi_i^\dagger}$ for the former harmonic function. From finite element fashion, the modal approach appears as a Petrov–Galerkin projection on high dimensional space where the trial functions are the harmonic modes and the test functions are the adjoint modes.

The steps necessary to derive the system of ODEs, which describes the reactor spatial dynamics according to the MM approach, are the following:

1. compute N eigenfunctions $\underline{\psi_i}$ from Eq. (9);
2. compute N adjoint eigenfunctions $\underline{\psi_i^\dagger}$ from the adjoint problem;
3. flux $\underline{\Phi}$ is approximated as

$$\underline{\Phi} \simeq \sum_{i=1}^{N} \underline{\underline{\psi_i}}\, \underline{a_i}(t), \tag{11}$$

where

$$\begin{cases} \underline{\underline{\psi_i}} = \begin{bmatrix} \psi_i^1(\mathbf{r}) & 0 \\ 0 & \psi_i^2(\mathbf{r}) \end{bmatrix}, \\ \underline{a_i}(t) = \begin{bmatrix} a_i^1(t) \\ a_i^2(t) \end{bmatrix}; \end{cases} \tag{12}$$

4. substitute the expression of Eq. (11) into Eqs. (1) and (2);
5. pre-multiply Eq. (1) by $\underline{\psi_j^\dagger}$ and Eq. (2) by $\underline{\psi_j^\dagger} \underline{\chi_d}$;
6. integrate over the spatial domain Ω.

Finally, for Eqs. (7) and (8), the following parameters have been obtained:

$$\begin{cases} \underline{\underline{\tau}}_{ji} = \int_\Omega \underline{\underline{\psi}}_j^\dagger \underline{\underline{V^{-1}}} \underline{\underline{\psi}}_i d\Omega, \\ \underline{\underline{A}}_{ji} = \int_\Omega \underline{\underline{\psi}}_j^\dagger \left[\nabla \cdot \underline{\underline{D}} \nabla - \underline{\underline{\Sigma}}_a - \underline{\underline{\Sigma}}_s\right] \underline{\underline{\psi}}_i d\Omega, \\ \underline{\underline{F}}_{p,ji} = \int_\Omega \underline{\underline{\psi}}_j^\dagger \underline{\underline{\chi}}_p \underline{\underline{F}}^T \underline{\underline{\psi}}_i d\Omega, \\ \underline{\underline{C}}_{mj} = \int_\Omega \underline{\underline{\psi}}_j^\dagger \underline{\underline{\chi}}_d C_m d\Omega, \\ \underline{\underline{F}}_{d,ji} = \int_\Omega \underline{\underline{\psi}}_j^\dagger \underline{\underline{\chi}}_d \underline{\underline{F}}^T \underline{\underline{\psi}}_i d\Omega. \end{cases} \tag{13}$$

It is worth mentioning that for such approach, the number of eigenfunctions needed to represent the quantities of interest with a certain level of accuracy for a given perturbed reactor configuration cannot be evaluated *a priori* (i.e., before the eigenfunctions are computed) nor *a posteriori* (i.e., once the eigenfunctions have been computed).

4. POD-based approach

As stated in the Introduction, the Proper Orthogonal Decomposition (POD) is a reduction order technique aimed at obtaining the most characteristic structure of the problem – the POD modes – using a low-dimensional approximate description of a high-dimensional process (Quarteroni et al., 2011). In this work, the POD modes have been computed relying on the snapshots technique (Sirovich, 1987). A snapshot is the solution of the high-order problem for a given combination of parameters, if any, and/or the solution at a determined integration time. Indeed, the POD builds the best orthonormal basis functions, in the least square sense, for the space spanned by the retained snapshots (Quarteroni et al., 2011), which form the so-called vector of the snapshots. Therefore, since the shape of the POD modes relies on the information present in the vector of the snapshots, the POD basis can be *trained* to reproduce specific configurations including their solution in the vector of the snapshots. In this way, the computational burden can be split into a demanding off-line phase, where the snapshots and the POD modes are computed, and into an inexpensive on-line phase where the reduced system is solved. The procedure for computing the POD modes can be summarized in the following steps (Volkwein, 1999):

1. compute N_s snapshots $\omega_1, \ldots, \omega_{N_s}$;
2. build the vector of the snapshots $\underline{X} = [\omega_1, \ldots, \omega_{N_s}]$;
3. perform the Singular Value Decomposition (SVD) on $\underline{X}$, so as to obtain:

$$\underline{X} = \underline{U}\ \underline{S}\ \underline{V}.$$

Once the SVD is executed, the columns of the matrix $\underline{U}$, $\underline{u}_i$, are the POD orthonormal modes, while the singular values, s_i, associated to each mode are sorted in descending order in the diagonal matrix $\underline{S}$. The singular value is proportional to the energy of each mode (i.e., to the information carried by the mode itself). In this work, the snapshots have been computed solving the generalized eigenvalue problem (9), and the number of retained snapshots is equal to one hundred. The values of $\underline{D}$, $\underline{\Sigma}_a$, and $\underline{\Sigma}_s$ have been perturbed within the spatial regions of the two irradiation channels (C.T. and RABBIT, see Fig. 1), to *train* the POD basis to handle such kind of perturbations, because, as reported in Section 6, they will be object of study. The values of the perturbed neutronic parameters have been randomly sampled in the range defined by their nominal values corresponding to water and void. For example, the absorption cross sections are sampled in the range defined as follows:

$$\underline{\underline{\Sigma}}_a \in \left[\underline{\underline{\Sigma}}_a(\text{void}), \underline{\underline{\Sigma}}_a(\text{water})\right]. \tag{14}$$

Once Eqs. (1) and (2) are projected onto the POD basis, the same functional forms of Eqs. (7) and (8) are obtained in which the following parameters have been employed:

$$\begin{cases} \underline{\underline{\tau}}_{ji} = \int_\Omega \underline{u}_j \underline{\underline{V^{-1}}} \underline{u}_i d\Omega, \\ \underline{\underline{A}}_{ji} = \int_\Omega \underline{u}_j \left[\nabla \cdot \underline{\underline{D}} \nabla - \underline{\underline{\Sigma}}_a - \underline{\underline{\Sigma}}_s\right] \underline{u}_i d\Omega, \\ \underline{\underline{F}}_{p,ji} = \int_\Omega \underline{u}_j \underline{\underline{\chi}}_p \underline{\underline{F}}^T \underline{u}_i d\Omega, \\ \underline{\underline{C}}_{mj} = \int_\Omega \underline{u}_j \underline{\underline{\chi}}_d C_m d\Omega, \\ \underline{\underline{F}}_{d,ji} = \int_\Omega \underline{u}_j \underline{\underline{\chi}}_d \underline{\underline{F}}^T \underline{u}_i d\Omega. \end{cases} \tag{15}$$

Differently from the Modal Method, the POD approach ensures an *a posteriori* estimate about the amount of information stored in the POD basis, defined by the following criterion (Atwell and King, 2004):

$$\frac{\sum_{i=1}^{e} s_i}{\sum_{i=1}^{N_s} s_i} > E, \tag{16}$$

where e provides an estimate of the number of basis functions necessary for an approximation with a desired mean square error less than $(1-E)\sum_{i=1}^{N_s} s_i$. In this way, the e modes retain $E \cdot 100$ percent of the information stored in the vector of the snapshots $\underline{X}$.

5. Reactivity evaluation by means of the Inverse Method

In Section 1, it has been stated that the developed approaches allow getting the system spatial dynamics, in addition to the time-dependent one, in order to monitor the evolution during operational transients of quantities of interest. Conversely, the most relevant output variable that allows the operator to effectively programme the control rod motion is the system reactivity, whose value determines the time-dependence of the externally imposed reactivity to yield a certain power variation. Therefore, from a control and safety oriented perspective, it is fundamental to evaluate the contribution of the several reactivity feedbacks.

Indeed, the perturbation performed on the system will be localized to a certain zone of the core. According to the position, the reactivity variation will be different, and the model should get these aspects and predict how the perturbation will extend to other core regions, reproducing these spatial dynamics effects. In the present work, the evaluation of the reactivity has been derived by means of the Inverse Method (Duderstadt and Hamilton, 1976). After a brief description of the classical formulation, it will be indicated how the algorithm has been modified and related to the time-dependent variables of the Modal-based and the POD-based approaches.

The Inverse Method refers to the following system of non-linear equations constituting the PK model:

$$\frac{\mathrm{d}\Psi}{\mathrm{d}t} = \frac{\rho(t) - \beta}{\Lambda}\Psi + \sum_{m=1}^{8} \frac{\beta_m}{\Lambda}\eta_m, \tag{17}$$

$$\frac{\mathrm{d}\eta_m}{\mathrm{d}t} = \lambda_m \Psi - \lambda_m \eta_m. \tag{18}$$

The state of the system is represented by the following normalized variables:

$$\Psi(t) = \frac{P(t)}{P(0)}, \tag{19}$$

$$\eta_m(t) = \frac{C_m(t)}{C_m(0)}, \tag{20}$$

whose initial conditions are defined as $\eta_m(0) = 1$ and $\Psi(0) = 1$. By substituting the analytical solution of precursor concentration into Eq. (17), it is possible to write:

$$\frac{d\Psi}{dt} = \frac{\rho(t)-\beta}{\Lambda}\Psi + \sum_{m=1}^{8}\frac{\beta_m}{\Lambda}\left[e^{-\lambda_m t} + \int_0^t \left[\lambda_m \Psi(t') e^{\lambda_m (t'-t)}\right] dt'\right]. \quad (21)$$

Once defined the delay quantity $\tau = t - t'$ and identified the "delayed neutron kernel" as:

$$D(\tau) = \sum_{m=1}^{8}\left(\frac{\lambda_m \beta_m}{\beta}\right) e^{-\lambda_m \tau},$$

it is possible to rearrange Eq. (21), obtaining an integro-differential form of the reactor point kinetics:

$$\rho(t) = \beta + \frac{\Lambda}{\Psi(t)}\frac{d\Psi}{dt} - \frac{1}{\Psi(t)}\sum_{m=1}^{8}\beta_m e^{-\lambda_m t} + - \frac{\beta}{\Psi(t)}\int_0^t D(\tau)\Psi(t-\tau)d\tau. \quad (22)$$

This expression indicates that by properly combining the PK equations it is possible to get an expression of the overall system reactivity, $\rho(t)$, as a function of the normalized power $\Psi(t)$. Given this result, the classical formulation of the Inverse Method has been extended, starting from the outcomes provided by the Modal and POD approaches. First of all, the expression of the thermal power density can be expressed as:

$$q'''(\mathbf{r},t) = \sum_l w_f^{(l)} N_l(\mathbf{r}) \int_0^\infty \sigma_f^{(l)}(E)\Phi(\mathbf{r},E,t)dE, \quad (23)$$

where l refers to the l-th fissile isotope, $w_f^{(l)}$ is the recoverable energy for each isotope fission event, $N_l(\mathbf{r})$ is the isotope density, $\sigma_f^{(l)}(E)$ is the microscopic fission cross section for the l-th isotope, $\Phi(\mathbf{r},E,t)$ is the neutron flux as function of position, energy and time. In the developed model, two neutron energy groups have been taken into account. Therefore, in Eq. (23) the integral is substituted by the following expression:

$$q'''(\mathbf{r},t) = \sum_l w_f^{(l)} N_l(\mathbf{r}) \cdot \left[\sigma_{f_1}^{(l)}(E)\Phi_1(\mathbf{r},t) + \sigma_{f_2}^{(l)}(E)\Phi_2(\mathbf{r},t)\right]. \quad (24)$$

After having obtained the fission macroscopic cross section for the considered domain, by integrating the expression (24) on the fuel pins volume, it possible to derive the value of the overall thermal power produced as follows:

$$P(t) = w_f \cdot \int_V \left[\Sigma_f^1(E)\Phi_1(\mathbf{r},t) + \Sigma_f^2(E)\Phi_2(\mathbf{r},t)\right] dV. \quad (25)$$

According to the presented approaches, the thermal and fast neutron fluxes have been expressed as a series of suitably defined functions in the form:

$$\Phi_1(\mathbf{r},t) = \sum_{i=1}^{N} b_i^1(\mathbf{r}) a_i^1(t), \qquad \Phi_2(\mathbf{r},t) = \sum_{i=1}^{N} b_i^2(\mathbf{r}) a_i^2(t). \quad (26)$$

By substituting these expressions in Eq. (25), the instantaneous value of the thermal power produced in the reactor core is achieved:

$$P(t) = w_f \cdot \sum_{i=1}^{N}\left[a_i^1(t)\cdot\langle\Sigma_f^1|b_i^1\rangle_V + a_i^2(t)\cdot\langle\Sigma_f^2|b_i^2\rangle_V\right]. \quad (27)$$

The terms $\langle\Sigma_f^1|b_i^1\rangle_V$ and $\langle\Sigma_f^2|b_i^2\rangle_V$ of the summation are evaluated off-line, while the $a_i^1(t)$ and $a_i^2(t)$ coefficients are computed by solving the developed ODE system defined by Eqs. (7) and (8). In order to derive the normalized power $\Psi(t)$, represented by Eq. (19), it is necessary to refer $P(t)$ to the power at nominal conditions $P(0)$. In this work, it has been assumed $P(0) = 1 \cdot w_f$. Therefore, $\Psi(t)$ is simply given by:

$$\Psi(t) = \frac{P(t)}{P(0)} = \sum_{i=1}^{N}\left[a_i^1(t)\cdot\langle\Sigma_f^1|b_i^1\rangle_V + a_i^2(t)\cdot\langle\Sigma_f^2|b_i^2\rangle_V\right]. \quad (28)$$

By substituting $\Psi(t)$ into Eq. (22), the system reactivity ρ can be derived.

6. Results and discussion

The comparison of the outcomes provided by the MM and the POD approaches focuses on the capability of evaluating the reactivity and the neutron flux shape. The different considered reactor configurations are the following:

(i) both the irradiation channels are empty (nominal configuration,[2] unperturbed);
(ii) water in the central channel, the RABBIT is empty;
(iii) water in the RABBIT, the central one is empty;
(iv) absorption cross sections have been homogeneously reduced by 3‰.

The above mentioned configurations, which are shown in Fig. 5, have been chosen in order to test the reliability and accuracy of the two approaches on the basis of both localized perturbations (Cases ii and iii) and homogeneous perturbation (Case iv). The POD basis has been trained with localized perturbations on the two irradiation channels, hence it is expected that the POD approach leads to high-fidelity results for Cases (ii and iii). On the other hand, the MM approach is likely to give good results for a homogeneous perturbation. The Cases (ii and iii) have been selected in order to asses if the two approaches manage to take into account spatial effects. Indeed, the same perturbation (i.e., void is replaced by water) is applied to different positions of the core where the neutron flux importance is different. Hence, the reactivity values are expected to be different in these two cases.

6.1. Methodology

For each configuration, an eigenvalue calculation – see Eq. (9) – has been performed by means of the open source finite element code freeFEM++ (Pironneau et al., 2012) relying on the ARPACK packages (Lehoucq et al., 1998), which implement an efficient implicit Arnoldi procedure, and on the MUltifrontal Massively Parallel sparse direct Solver (MUMPS) (Amestoy et al., 2000). The obtained reactivity value and flux shape will be referred to as *reference* solution.

Subsequently, using the MATLAB/Simulink environment (MATLAB® and SIMULINK® software, 2005), the evolution of the system described by Eqs. (7) and (8), within the first 60 s, has been simulated according to the MM and POD approaches. The reactivity has been estimated by means of the described procedure of the Inverse Method (Section 5) after infinite time elapsed subsequent the step reactivity insertion. In order to compare the computed flux shapes with the reference one, which is time-independent, the former, at the end of the simulation, are normalized as follows:

$$\int_\Omega (\Phi_1 + \Phi_2) d\Omega = 1. \quad (29)$$

A sensitivity analysis for the outcomes provided by the MM and POD approaches has been carried out varying the number of basis functions up to 100. For the sake of completeness, the trivial case with only one basis function has been considered as well, showing the necessity of allowing for an increased number of modes.

[2] The eigenfunctions of the MM have been computed for this configuration.

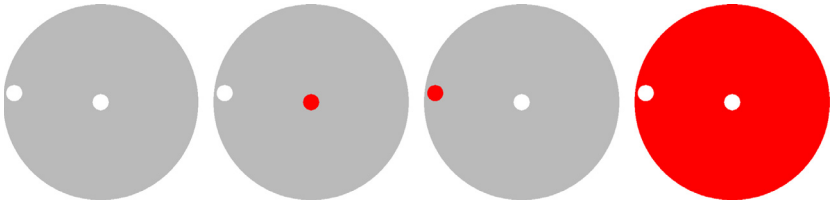

Fig. 5. The four reactor configurations simulated. The perturbed areas, with respect to nominal configuration (Case i), are highlighted in red. (For interpretation of the references to colour in this figure legend, the reader is referred to the web version of this article.)

In the following, the outcomes of the two approaches, for each reactor configuration, will be presented and discussed.

6.2. Case i: unperturbed configuration

This case is the nominal configuration (unperturbed) of the reactor. According to the two approaches, the estimated values of reactivity, varying the number of basis functions, are reported in Table 3, and they are graphically compared in Fig. 6. The POD prediction, if the basis is made of only the first function, is very far from the reference value but it gets closer when two and three functions are used. If four or more functions are employed, the value of the reactivity does not change anymore. Even increasing the number of functions employed, the reactivity values estimated by means of the MM approach does not change, since the reference flux shape is precisely the first eigenfunction of each group. The flux shape of the energy group 2 (from now on referred to as thermal group) given by the two approaches is compared to the reference one in Fig. 7. In particular, the reference flux shape (a), POD (b) using 4 functions, and MM (c) employing 10 eigenfunctions are depicted. The MM flux shape is coincident with the reference one, while the POD flux shape is very close.

6.3. Case ii: water in the central channel

This kind of perturbation may be considered as the worst case, since the perturbation is quite localized in a position where the neutron importance is higher. The reactivity values provided by the two approaches, employing different number of basis functions, are reported in Table 4, and the chart shown in Fig. 8 compares the results. The POD prediction, if the basis is made of only the first function, is very far from the reference value but it gets

Table 3
Reactivity calculations for the configuration corresponding to Case i.

# Of functions	Reactivity (pcm)		
	Reference	POD	MM
1	0	−765.3	4.5
2	0	−14.7	4.5
3	0	−0.7	4.5
4	0	0.8	4.5
5	0	0.8	4.5
6	0	0.8	4.5
7	0	0.8	4.5
8	0	0.8	4.5
9	0	0.8	4.5
10	0	0.8	4.5
50	0	0.8	4.5
100	0	0.8	4.5

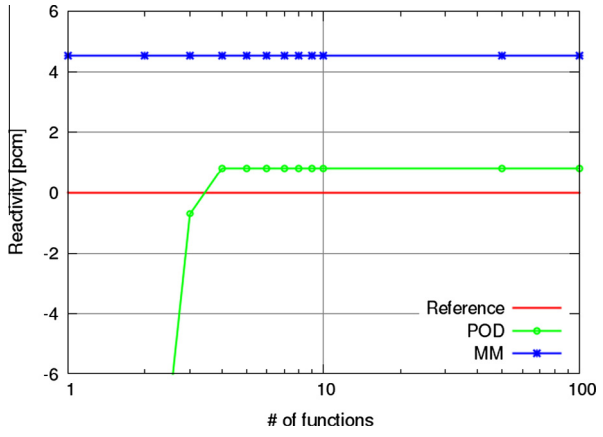

Fig. 6. Reactivity calculations for the configuration corresponding to Case i.

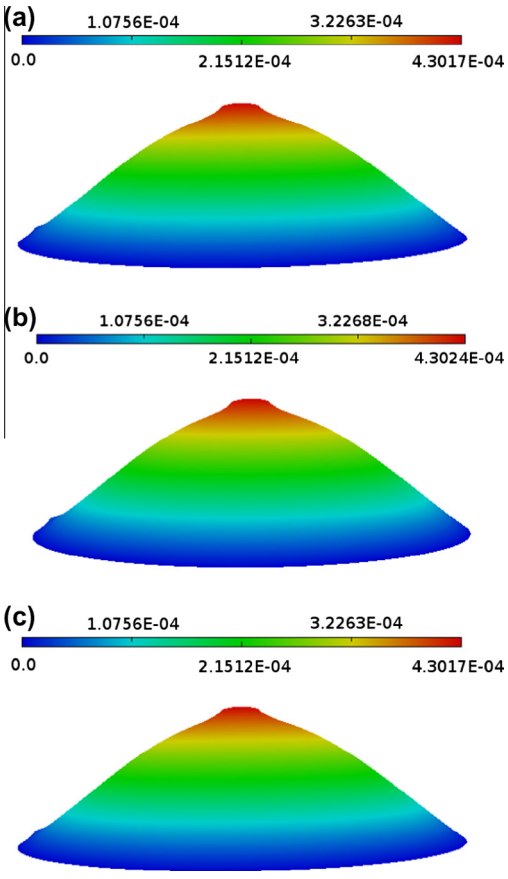

Fig. 7. Thermal flux shape for Case i: reference (a), POD (b), and MM (c). Data are reported in arbitrary units.

Table 4
Reactivity calculations for the configuration corresponding to Case ii.

# Of functions	Reactivity (pcm)		
	Reference	POD	MM
1	166.4	650.4	365.2
2	166.4	155.6	365.2
3	166.4	167.5	365.2
4	166.4	167.2	365.2
5	166.4	167.2	365.1
6	166.4	167.2	345.5
7	166.4	167.2	345.5
8	166.4	167.2	345.5
9	166.4	167.2	345.4
10	166.4	167.2	345.4
50	166.4	167.2	300.4
100	166.4	167.2	266.9

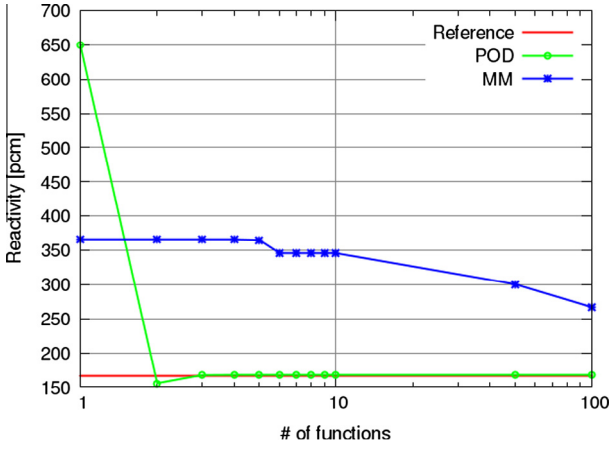

Fig. 8. Reactivity calculations for the configuration corresponding to Case ii.

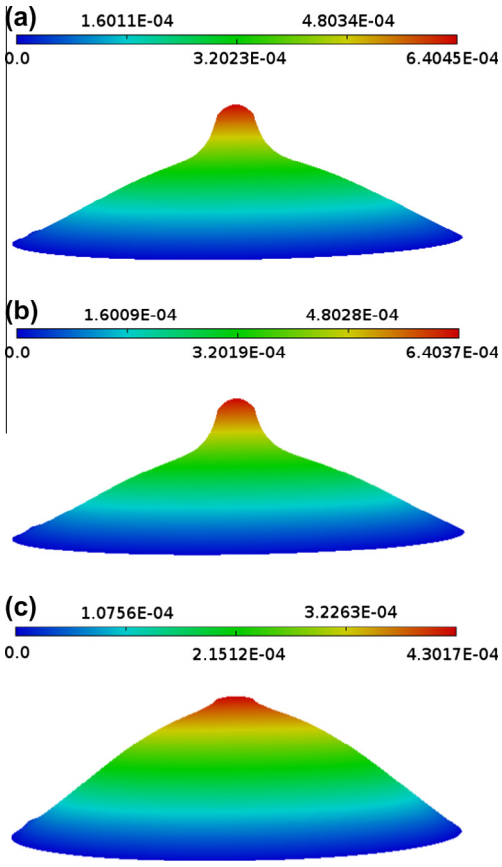

Fig. 9. Thermal flux shape for Case ii: reference (a), POD (b), and MM (c). Data are reported in arbitrary units.

closer when two and three functions are used. If four or more functions are employed, the value of the reactivity does not change anymore. The reactivity values estimated by means of the MM approach slightly converges to the reference value as the number of functions employed increases. This slight change is due to the fact that for such perturbation, only the odd eigenfunctions manage to reflect a change in the middle of the core, but the series of all eigenfunction does not inherit this property. As a result, even employing 100 eigenfunctions, the reactivity is overestimated by a factor of 1.6. Conversely, by employing only four POD functions, the reactivity differs from the reference value by 0.8 pcm, which is the offset when compared to the unperturbed configuration (Case i, see Table 3). In Fig. 9, the reference (a) flux shape, the one computed according to the POD approach (b) employing 4 functions, and according to the MM approach (c) using 10 functions, are represented. The MM approach cannot represent any flux shape variation if compared to the nominal configuration (see Fig. 7) – even though the estimated reactivity is more than twice the reference one. On the other hand, the flux shape computed by the POD approach fits very well the reference one.

6.4. Case iii: water in the RABBIT channel

In this test case, the same perturbation as in the previous Case (ii) is applied, but localized in a different position. In fact, the water is placed in the peripheral RABBIT channel, where the neutron importance is much lower compared to the middle of the reactor core. This leads to a lower reactivity change, in comparison with the previous case. The estimated reactivity, according to the two

Table 5
Reactivity calculations for the configuration corresponding to Case iii.

# Of functions	Reactivity (pcm)		
	Reference	POD	MM
1	3.4	−745.0	1.510
2	3.4	7.5	1.505
3	3.4	3.6	1.505
4	3.4	4.2	1.504
5	3.4	4.2	1.490
6	3.4	4.2	1.502
7	3.4	4.2	1.490
8	3.4	4.2	1.485
9	3.4	4.2	1.485
10	3.4	4.2	1.468
50	3.4	4.2	0.985
100	3.4	4.2	0.577

approaches, varying the number of functions employed, is reported in Table 5, and the corresponding chart is shown in Fig. 10. The POD prediction behaves as discussed in the previous cases. Indeed, if the basis is made of only the first function, the outcome is quite different from the reference value, while with four or more basis functions employed the value of the reactivity does not change anymore. The difference between the prediction of the POD approach differs by 0.8 pcm with respect to the reference value, which is the offset when compared to the unperturbed configuration (Case i, see Table 3). The reactivity values estimated by means of the MM approach barely change by increasing the number of functions employed, but the trend seems to be divergent in comparison with the reference value. If the entity of this perturbation,

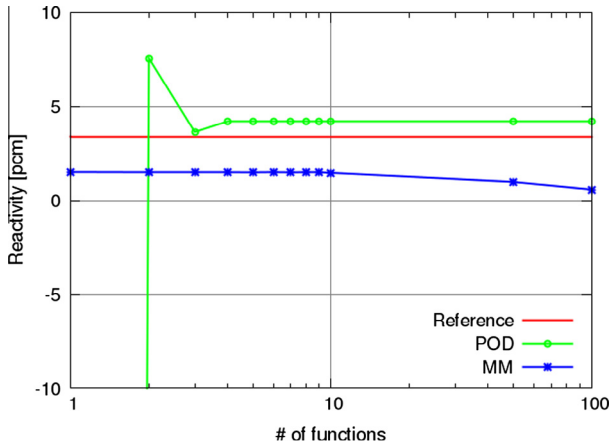

Fig. 10. Reactivity calculations for the configuration corresponding to Case iii.

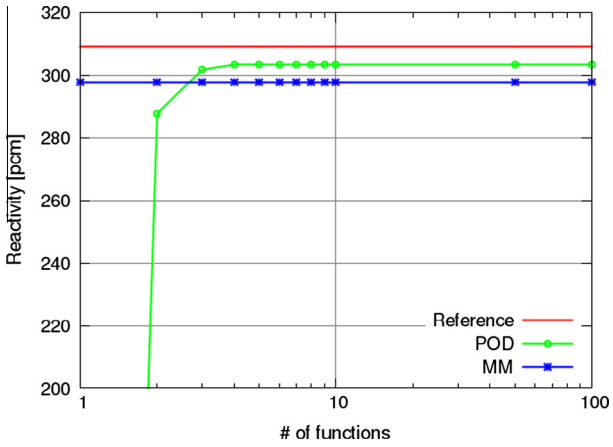

Fig. 11. Reactivity calculations for the configuration corresponding to Case iv.

in terms of reactivity, is compared to the previous one, it can be deduced that both the two approaches effectively reproduce the system spatial effects. Indeed, both the methods have provided a bigger reactivity change, with respect to the unperturbed configuration, when the perturbation is applied in the center of the core. Otherwise, a smaller effect has been seen when the same perturbation is applied where the importance of the neutron flux is much lower.

In this case, the flux shape variation is small, hence it is not worthy to show the neutron fluxes provided by the two approaches.

6.5. Case iv: homogeneous perturbation

In this case, a homogeneous perturbation throughout the core is simulated by reducing the absorption cross sections by 3‰. According to the two approaches, the computed reactivity values, varying the number of basis functions, are given in Table 6, and they are graphically compared in Fig. 11. Also for this kind of perturbation, the outcomes provided by the POD approach are not accurate when only one basis function is employed. If four or more modes are adopted, the reactivity value is closer to the reference one and it does not change anymore by increasing the number of functions. The estimation of the reactivity provided by the MM does not change sensitively by increasing the number of functions employed. However, the outcomes of both approaches are in fair agreement with the reference value.

Table 6
Reactivity calculations for the configuration corresponding to Case iv.

# Of functions	Reactivity (pcm)		
	Reference	POD	MM
1	309.0	−462.6	297.936
2	309.0	287.8	297.936
3	309.0	301.8	297.936
4	309.0	303.3	297.936
5	309.0	303.3	297.936
6	309.0	303.3	297.936
7	309.0	303.3	297.935
8	309.0	303.3	297.935
9	309.0	303.3	297.935
10	309.0	303.3	297.935
50	309.0	303.3	297.935
100	309.0	303.3	297.935

As in the previous test case (Case iii), the homogeneous perturbation does not change significantly the flux shape, hence the neutron fluxes provided by the two approaches are not worthy of remarks.

6.6. Discussion

The comparison between the presented control-oriented approaches for the nuclear reactor kinetics has been performed on different reactor configurations.[3] Whether a homogeneous perturbation is evaluated (Case iv), both the approaches exhibit good capabilities to approximate the flux shape. On the other hand, if the perturbation is localized, the MM requires a considerable number of eigenfunctions to correctly predict the reactivity. Moreover, the flux shape predicted according to the MM does not reflect the localized perturbation. Conversely, the outcomes provided by the POD approach, employing only four basis functions, are high-fidelity with respect to the reference ones, in terms of reactivity and flux shape, independently on the kind of applied perturbation.

The motivation of the better results obtained by POD are due to the difference between the shape of the corresponding POD (Fig. 12) and MM (Fig. 13) basis functions, where for brevity only the first four modes for the thermal group are shown. The first POD function (starting from the left) provides the overall flux shape, while the higher order functions give contributions only where the perturbations can be applied. Such shape reflects the *training* that has been performed to compute the POD basis. On the other hand, the shape of the MM functions depends on the operators $\mathcal{L}$ and $\mathcal{M}$ of the generalized eigenvalue Eq. (10) and on the geometry of the unperturbed core. Therefore, the MM basis has no information where the perturbations may occur.

For each case considered, the outcomes provided by the POD approach behave in the same way. In particular, if a single basis function is employed, the reactivity value is quite far from the reference one, whereas it gets closer when two and three functions are used. If four or more functions are employed, the value is in good agreement with the reference one and does not change anymore. Indeed, the importance of contribution given by each POD function is decreasing, meaning that the next function carries less information (or energy) than the previous one. The energy associated to each POD function is shown in Fig. 14. The difference

[3] The considered reactor core configurations have been achieved starting from an unperturbed configuration, to which either localized or homogeneous perturbations have been applied.

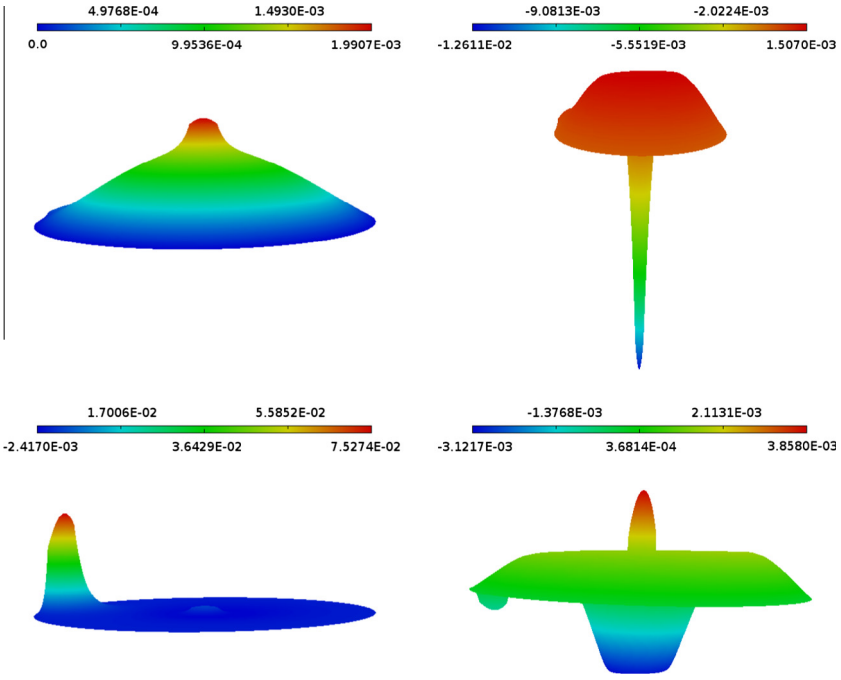

Fig. 12. The first four POD basis functions for the thermal group.

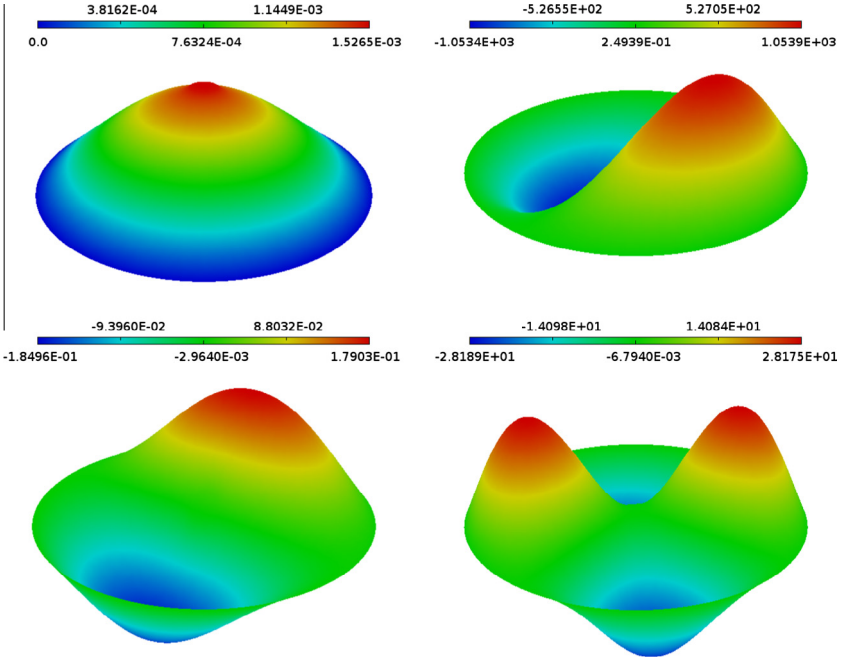

Fig. 13. The first four MM basis functions for the thermal group.

between the first and the fourth value is equal to several orders of magnitude. This means that the information stored in the vector of the snapshots can be reproduced by only few functions. Relying on the *a posteriori* criterion, Eq. (16), the retained information, expressed in percent, with respect to the number of functions employed, is reported in Fig. 15. It can be seen that with two basis functions more than the 99% of the information stored in the vector of the snapshots is allowed for, and with four functions all the information is reproduced. Hence, the contribution of the functions beyond the fourth one is negligible. For this reason, the outcomes, obtained employing more than four functions, do not change considerably.

Conversely, the outcomes provided by the MM approach behave differently in the considered cases. In particular, for the unperturbed configuration, the quantities of interest do not change by increasing the number of functions. For Case (ii), as the number of modes is increased, the reactivity value slightly converges to the reference value. In Case (iii), although the reactivity value is close to the reference one, there is a divergent trend. Finally, when a homogeneous perturbation is applied (Case iv), the reactivity

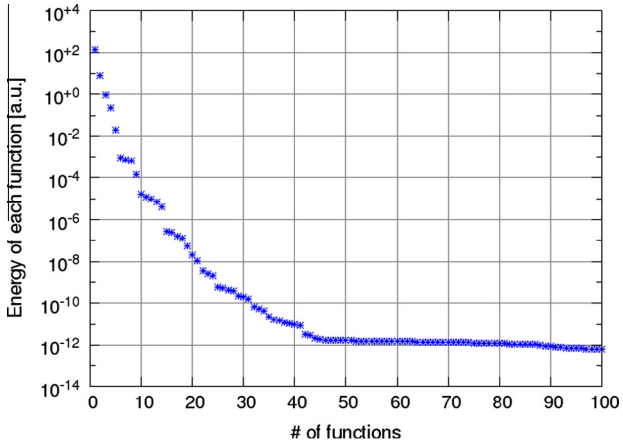

Fig. 14. Energy of POD functions for the thermal group.

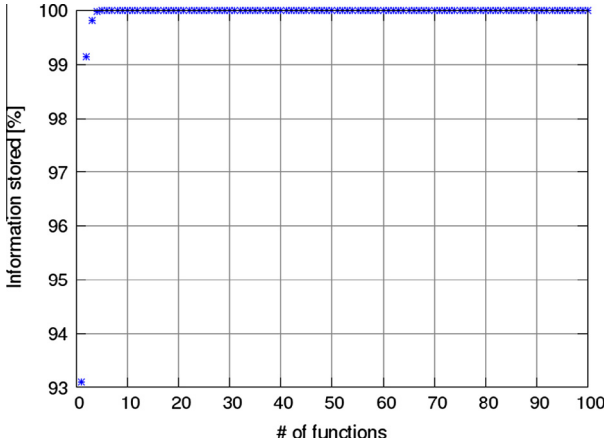

Fig. 15. Relative information taken into account with respect to the number of functions employed for the POD spatial basis.

value does not change by increasing the number of functions. The importance of each eigenfunction depends on the kind of perturbation, and it cannot be provided neither *a priori* nor *a posteriori* estimation. For example, in the Case (ii), only the odd eigenfunctions can contribute to reveal a change in the middle of the core.

7. Conclusions

In this paper, two control-oriented modelling approaches, based on a Modal Method (MM) and on the Proper Orthogonal Decomposition (POD) technique, for the nuclear reactor kinetics have been presented and compared. Both are able to simulate the spatial dynamics of the reactor, while the usually adopted point-wise kinetics is not sensible to spatial effects. In order to asses the reliability of these two approaches, different reactor core perturbations have been simulated, with reference to the TRIGA Mark II reactor of the University of Pavia. In particular, either localized or homogeneous perturbations have been investigated. The system reactivity and the neutron flux shape predicted by the MM and POD approaches have been the main focus for the comparison. The outcomes provided by the POD approach, employing as few as four basis functions, are high-fidelity, with respect to the reference ones, for all the cases considered. Conversely, the MM approach leads to good results when the perturbation is homogeneous. On the other hand, if the perturbation is localized, a considerable number of eigenfunctions may be required to correctly predict the reactivity.

The presented work is meant to be a preliminary investigation on the adoption of these two approaches in order to find the right track to be pursued in the future. The TRIGA reactor modelling will be improved in order to provide results that can be assessed with collected experimental data. In this perspective, a more detailed core geometry (e.g., 3D modelling) along with a neutronic description using four energy groups will be developed. In addition, the modelling of the thermal-hydraulics phenomena is foreseen. Finally, in order to avoid the presence of redundant information, which may occur whether the adopted random sampling is carried out, a more efficient sampling of the snapshots will be investigated. The possibility of employing different reduced order methods, such as reduced basis (see e.g., Manzoni et al., 2012), in a many-query framework (e.g., multi-physics and multi-scale modelling) is envisaged as well.

Acknowledgements

The authors wish to express their thanks to Prof. Alfio Quarteroni (CMCS, École Polytechnique Fédérale de Lausanne), Prof. Luca Formaggia (MOX), Prof. Hisashi Ninokata (CeSNEF), and Stefano Lorenzi (CeSNEF) for their active interest and stimulating conversation on the subject of this paper and its future perspectives.

References

Amestoy, P.R., Duff, I.S., L'Excellent, J.Y., 2000. Multifrontal parallel distributed symmetric and unsymmetric solvers. Comput. Methods Appl. Mech. Eng. 184, 501–520.
Ascher, U.M., Petzold, L.R., 1997. Computer Methods for Ordinary Differential Equations and Differential–Algebraic Equations. SIAM.
Atwell, J., King, B., 2004. Reduced order controllers for spatially distributed systems via proper orthogonal decomposition. SIAM J. Sci. Comput. 26, 128–151.
Aufiero, M., Cammi, A., Fiorina, C., Luzzi, L., Sartori, A., 2013. A multi-physics time-dependent model for the Lead Fast Reactor single-channel analysis. Nucl. Eng. Des. 256, 14–27.
Buchan, A., Pain, C., Fang, F., Navon, I., 2013. A POD reduced-order model for eigenvalue problems with application to reactor physics. Int. J. Numer. Methods Eng..
Cammi, A., Di Marcello, V., Luzzi, L., Memoli, V., Ricotti, M.E., 2011. A multi-physics modelling approach to the dynamics of Molten Salt Reactors. Ann. Nucl. Energy 38, 1356–1372.
Chatterjee, A., 2000. An introduction to the proper orthogonal decomposition. Curr. Sci. 78, 808–817.
Duderstadt, J.J., Hamilton, L.J., 1976. Nuclear Reactor Analysis. John Wiley & Sons, New York.
General Atomic, 1964. TRIGA Mark II Reactor General Specifications and Description. General Atomic Company, USA.
GIF, 2002. A Technology Roadmap for Generation IV Nuclear Energy System. Technical Report. GIF-002-00.
Holmes, P., Lumley, J., Berkooz, G., 1996. Turbolence, Coherent Structures, Dynamical Systems and Symmetry. Cambridge University Press.
Koning, A., Forrest, R., Kellett, M., Mills, R., Henriksson, H., Rugama, Y., 2006. The JEFF-3.1 Nuclear Data Library. Technical Report NEA – OECD, JEFF Report 21.
Lehoucq, R.R.B., Sorensen, D.D.C., Yang, C.C., 1998. Arpack User's Guide: Solution of Large-Scale Eigenvalue Problems with Implicitly Restorted Arnoldi Methods, vol. 6. SIAM.
Liang, Y., Lee, H., Lim, S., Lin, W., Lee, K., Wu, C., 2002. Proper orthogonal decomposition and its applications–Part I: Theory. J. Sound Vib. 252, 527–544.
Manzoni, A., Quarteroni, A., Rozza, G., 2012. Computational reduction for parametrized PDEs: strategies and applications. Milan J. Math. 80, 283–309.
MATLAB® and SIMULINK® software, 2005. The MathWorks, Inc.
Merzari, E., Ninokata, H., 2011. Proper orthogonal decomposition of the flow in a tight lattice rod-bundle. Nucl. Eng. Des. 241, 559–572.
Pearson, K., 1901. On lines and planes of closest fit to system of points in space. Philos. Mag. 2, 559–572.
Pironneau, O., Hecht, F., Morice, J., 2012. freeFEM++, v3.19. <http://www.freefem.org/ff++>.
Prill, D., Class, A., 2014. Semi-automated proper orthogonal decomposition reduced order model non-linear analysis for future BWR stability. Ann. Nucl. Energy 67, 70–90.
Quarteroni, A., Rozza, G., Manzoni, A., 2011. Certified reduced basis approximation for parametrized partial differential equations and applications. J. Math. Ind. 1, 1–49.

Quarteroni, A., Valli, A., 2008. Numerical Approximation of Partial Differential Equations, vol. 23. Springer.
Rozza, G., Huynh, D., Patera, A., 2008. Reduced basis approximation and a posteriori error estimation for affinely parametrized elliptic coercive partial differential equations. Arch. Comput. Methods Eng. 15, 1–47.
Schultz, M.A., 1961. Nuclear Reactor Kinetics and Control. McGraw-Hill.
SERPENT, 2011. PSG2/Serpent Monte Carlo Reactor Physics Burnup Calculation Code. <http://montecarlo.vtt.fi>.
Sirovich, L., 1987. Turbulence and the dynamics of coherent structures. I–III. Quart. Appl. Math. 45, 561–590.
Stacey, W.M., 1969. Space–Time Nuclear Reactor Kinetics. Academic Press.
Volkwein, S., 1999. Proper Orthogonal Decomposition and Singular Value Decomposition. Karl-Franzens-Universität Graz & Technische Universität Graz.
Wols, F., 2010. Transient Analyses of Accelerator Driven Systems using Modal Expansion Techniques, M.S. Thesis, Delft University of Technology.
Xia, L., Jiang, J., Javidnia, H., Luxat, J.C., 2012. Performance evaluation of a 3-D kinetic model for CANDU reactors in a closed-loop environment. Nucl. Eng. Des. 243, 76–86.